Hindawi
International Journal of Antennas and Propagation
Volume 2017, Article ID 8215291, 8 pages
https://doi.org/10.1155/2017/8215291

Research Article

Transmission Control of Electromagnetic Waves by Using Quarter-Wave Plate and Half-Wave Plate All-Dielectric Metasurfaces Based on Elliptic Dielectric Resonators

Ali Yahyaoui,[1,2] Hatem Rmili,[1,3] Karim Achouri,[4] Muntasir Sheikh,[3] Abdullah Dobaie,[3] Adnan Affandi,[3] and Taoufik Aguili[1]

[1] *University of Tunis El Manar (UTM), National Engineering School of Tunis (ENIT), Communications Systems Laboratory (SysCom), BP 37, Belvédère, 1002 Tunis, Tunisia*
[2] *Electrical and Computer Engineering Department, University of Jeddah, P.O. Box 80327, Jeddah 21589, Saudi Arabia*
[3] *Electrical and Computer Engineering Department, King Abdulaziz University, P.O. Box 80204, Jeddah 21589, Saudi Arabia*
[4] *Department of Electrical Engineering, École Polytechnique de Montréal, Montréal, QC, Canada H3T 1J4*

Correspondence should be addressed to Ali Yahyaoui; ali.yahyaoui@enit.utm.tn

Received 30 May 2017; Accepted 2 August 2017; Published 10 October 2017

Academic Editor: Paolo Burghignoli

We present the design of all-dielectric Quarter-Wave Plate (QWP) and Half-Wave Plate (HWP) metasurfaces based on elliptic dielectric resonators (EDRs) for the transmission control of electromagnetic waves over the frequency band 20–30 GHz. First, an extensive numerical analysis was realized by studying the effect of the resonators geometry (thickness and ellipticity) on the transmission of both x- and y-polarized waves. Then, based on the numerical analysis, we have realized and characterized experimentally both QWP and HWP all-dielectric metasurfaces.

1. Introduction

Metamaterials are artificial structures typically engineered by arranging a set of scattering elements in a regular pattern throughout a volumetric region of space. This arrangement allows for desirable bulk electromagnetic responses that are typically not found naturally. The extraordinary metamaterial control of electromagnetic waves is due to the possibility of engineering effective negative refractive index, near-zero index, cloaking materials, and so forth. Over the past several years, metamaterials have evolved from a theoretical concept to a mature and groundbreaking technology with real-world applications [1–5]. However, three-dimensional metamaterials suffer from major issues, such as high losses, bulkiness, and difficulty of fabrication. Most of these disadvantages may be eliminated by reducing their dimensionality by arranging electrically small scattering elements into a two-dimensional pattern at a surface or interface. This two-dimensional version of a metamaterial has been given the name metasurface [6, 7]. For many applications, metasurfaces can be used in place of metamaterials with the advantage of taking up less physical space and having lower losses.

When the electric and magnetic resonance frequencies of the dielectric resonators are different, the phase variation of the transmission coefficient is limited to π, whereas this value can reach 2π by superposition of both resonances at the same frequency [8].

Metasurfaces have a wide range of potential applications in electromagnetics including, but not limited to, controllable surfaces, miniaturized cavity resonators, novel wave-guiding structures, angular-independent surfaces, absorbers, biomedical devices, fast switches, and fluid-tunable frequency-agile materials. Recently, several experimental research works have been published on the realization of metasurfaces with such novel functionalities [9].

The spatial distribution of the subwavelength elements composing the metasurface acts on the incident wave in terms of amplitude, phase, and polarization, which may affect its electromagnetic response, and offers the possibility of obtaining specific functionalities.

However, the majority of metasurfaces were designed by using metallic elements with Ohmic losses, which may limit their performances especially at optical frequencies. In order to overcome these limitations, all-dielectric metasurfaces have attracted particular interest recently; and some successful designs with low-losses, high overall efficiency, and various functionalities [10–15] were obtained in microwave and optical frequencies.

Dielectric resonators are the main structure used in all-dielectric metasurfaces because they can excite both electric and magnetic resonant modes, in addition to the possibility of reducing the size by using high dielectric constant ε_r. Several resonators shapes such as spheres, cubes, cylindrical/elliptical disks, and rods were investigated in order to design all-dielectric metasurfaces especially at THz and optical frequencies [12–15].

Therefore, in all-dielectric metasurfaces based on dielectric resonators, the geometrical parameters of the resonators and the spacing between them are the main factors affecting the phase variation as well as the metasurface performances [16–18].

Recently, we are interested in the design of all-dielectric metasurfaces based on EDRs operating at microwave frequencies. The main design parameters of these resonators are their ellipticity, orientation, and thickness. In the first study [18], we have investigated numerically the effect of the resonators ellipticity and orientation on the metasurface transmission. In this paper, we propose a complementary study to first determine numerically, by using the Ansys-HFSS software, the effect of the resonators thickness. Then, we realize and characterize experimentally the optimized prototypes of the QWP and HWP metasurfaces.

2. Metasurface Design

The proposed all-dielectric metasurface consists of an infinite two-dimensional array of connected EDRs, as shown in Figure 1(a), made of dielectric (Rogers RO3210) of relative permittivity 10.2, loss tangent 0.003, and thickness h.

The minor (along x) and major radii (along y) of the EDR are denoted as a and b, respectively, whereas its ellipticity is $\tau = b/a$. The size of the unit cell is $L_x \times L_y \times L_z$. In this regard, $L_x = 9.9\,\text{mm}$ ($L_x < \lambda$), $L_y = 9.9\,\text{mm}$ ($L_y < \lambda$), and $L_z = 16\lambda$, where $\lambda = 10\,\text{mm}$ is the wavelength associated with the upper frequency limit 30 GHz, and the longitudinal dimension L_z is great compared to the wavelength λ ($L_z = 160\,\text{mm}$). The resonators are connected along x-direction with thin connection of length $L_c = (L_x/2) - b$ and width $W_c = 1.25\,\text{mm}$. We have excited the structure with normal incidence (Floquet ports) along z-direction.

The ellipticity of the resonator was studied by varying the ratio τ of EDRs while fixing the minor radius at $a = 2\,\text{mm}$ ($\lambda/5$), without affecting the cell size (τ is bounded within the ranges: $1 \le \tau \le 2.47$ with a step of 0.01). Finally, the height h of both the EDRs and the connections is varied from 0.64 to 2.56 mm with a step of 0.64 mm.

3. Simulated Results

The simulation of the metasurface was performed by using the commercial software Ansys-HFSS. In Figure 1(b), we present the simulation model where the unit cell boundary condition was used along x- and y-directions. The model is excited under normal incidence with Floquet ports along z-direction in the frequency range 20–30 GHz.

In order to study the transmission of the designed all-dielectric metasurface, we have analyzed its response when excited under normal incidence with two orthogonal polarization parallel to x- and y-axes as shown in Figure 1(a).

We define then $T_{xx} = |E_x{}^t|/|E_x{}^i|$ and $T_{yy} = |E_y{}^t|/|E_y{}^i|$ as the module transmission ratio of x- and y-linear polarization of the electric field, respectively, and $\Delta\phi = \phi_x - \phi_y$ as the phase difference between the x- and y-components of the transmitted electromagnetic fields. Consequently, the moduli T_{xx} and T_{yy} will vary from 0 to 1, and the phase difference $\Delta\phi$ varies from -360° to $+360^\circ$. The QWP and HWP metasurfaces are obtained when the moduli are equal ($T_{xx} = T_{yy}$) and the phase difference is $\Delta\phi = \pm 90^\circ$ and $\pm 180^\circ$, respectively.

3.1. Effect of the Resonator Geometry. We have investigated the effect of the main design parameters affecting the transmission of the all-dielectric metasurface, in particular the resonators thickness h, size, and shape (ellipticity τ). The effect of the resonator size on the metasurface transmission was studied mainly by varying the EDR major axis b. Results for radius $a = \lambda/5$ are illustrated in Figure 2. The effect of the EDR ellipticity on the metasurface transmission was analyzed from moduli (T_{xx} and T_{yy}), phases (ϕ_x and ϕ_y), the ratio between moduli (we take $\log(T_{xx}/T_{yy})$ for better visualization), and the phase shift $\Delta\phi$, for four considered resonator thicknesses $h_1 = 0.64\,\text{mm}$, $h_2 = 1.28\,\text{mm}$, $h_3 = 1.92\,\text{mm}$, and $h_4 = 2.56\,\text{mm}$.

In Figure 2, we have studied, over the frequency band 20–30 GHz, the effect of the resonator ellipticity τ and thickness h, on the metasurface transmission. We can remark easily that the exciting frequency and the resonators geometry (ellipticity and thickness) affect deeply the metasurface transmission behavior. We can notice also that ellipticity of the resonators affects more moduli and phases of y-polarized incident waves (ϕ_y) than x-polarized waves (ϕ_x) due to the orientation of the resonators along the y-axis.

However, by analysis of colors distribution in Figure 2(a), we can note that the red color, which represents high transmission moduli (T_{xx} and T_{yy}), is more dominant in graphs corresponding to metasurfaces excited with y-polarized waves. This result can be explained by the connection extension along the x-axis which reduces slightly the transmission along this direction.

From Figure 2(b), we can notice the equality between moduli represented with green color.

On the other hand, we can note that the phases ϕ_x and ϕ_y (Figure 2(c)) as well as the phase shift $\Delta\phi$ (Figure 2(d))

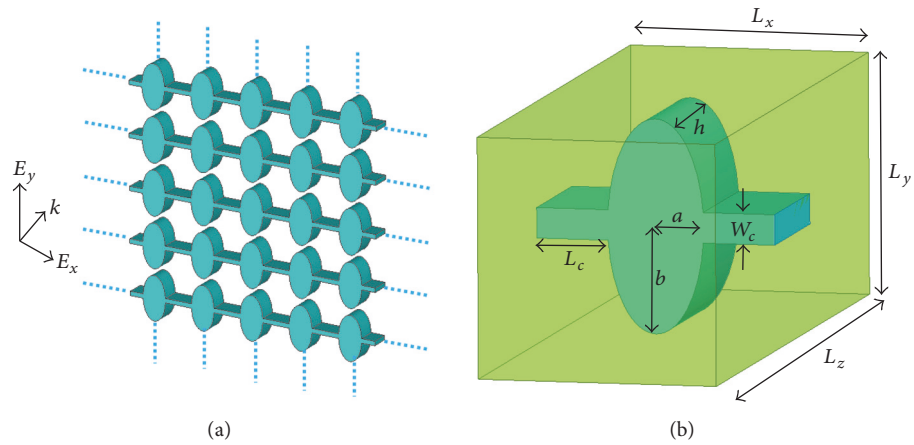

FIGURE 1: Schema of the proposed all-dielectric metasurface: (a) 2D connected EDR array with x- and y-polarization of the electric field and (b) HFSS-model for the unit cell.

variations are increased for higher values of the metasurface thickness h, which means that the phase difference $\Delta\phi$ spans a wider range of values for thick metasurfaces.

3.2. Application: QWP and HWP Metasurfaces. In order, to design all-dielectric QWP and HWP metasurfaces, we have considered the previous results of the parametric study (Section 3.1). Both of QWP and HWP metasurfaces require high transmission and particular phase shift ($|\Delta\phi| = 90^\circ$ for QWP and $|\Delta\phi| = 180^\circ$ for HWP). In Table 1, we have regrouped main data, deduced from Figure 2, related to the design of QWP and HWP devices. For each metasurface of thickness h (0.64 mm, 1.28 mm, 1.92 mm, and 2.56 mm), we have presented the bandwidths (column 2) associated with QWP and HWP metasurfaces where the transmissions moduli T_{xx} and T_{yy} (columns 3 and 4) are considered to be greater than 0.7 and the phase shift is $|\Delta\phi| = 90^\circ \pm 5^\circ$ for QWP (column 5) and $|\Delta\phi| = 180^\circ \pm 5^\circ$ for HWP (column 6); these results are obtained for ellipticity ranges given in column 7.

From Table 1, we can deduce that the transmission level of the x- and y-polarization (T_{xx} and T_{yy}) is increased with the thickness h; cases (where moduli > 0.9) are obtained with the thickness 2.56 mm. We can note also that, except for the thickness 1.28 mm, we can design QWP and HWP metasurfaces with good performances; however, only the thickness 2.56 mm allows us to design both QWP and HWP operating in different frequency ranges.

4. Experimental Validation

Two metasurface prototypes, each one composed of 7×7 cells, were fabricated with Rogers RO3210 substrates of thickness $h = 2.56$ mm ($\approx\lambda/3.8$), relative permittivity $\varepsilon_r = 10.2$, and loss tangent $\tan\delta = 0.0027$. The total thickness 2.56 mm was obtained by superposition of 4 identical layers, each one of thickness 0.64 mm. The unit cell size is 9.9 mm ($\approx\lambda$). The dielectric connections are oriented along x-direction as illustrated in Figure 3. The two devices were characterized by measuring their x- and y-polarized transmission coefficients in an anechoic room over the frequency band 20–30 GHz.

The first fabricated metasurface is a QWP structure (Figure 3(a)) designed to transmit both x- and y-polarization with phase shift difference $|\Delta\phi| \approx 90^\circ$ and equal moduli ($T_{xx} = T_{yy}$). The resonators ellipticity $\tau = b/a$ is equal to 1.46 ($\approx\lambda/6.7$), where the minor and major elliptic resonators radii are $a = 2$ mm ($\approx\lambda/5$) and $b = 2.92$ mm ($\approx\lambda/3.4$), respectively. The measured transmitted power, for both of x- and y-polarization, over the band 24–30 GHz, is given in Figure 4.

We have regrouped in Table 2 both simulated and measured results for the designed QWP and HWP metasurfaces. We can notice, from these results, that we have good agreement between simulation and measurement in terms of moduli and phase difference of the transmitted power, with a certain frequency shift attributed mainly to fabrication imperfections and error measurements.

We can notice, from Figure 4, that, at the frequency of 28.2 GHz, both x- and y-polarized transmission moduli are equal (≈−1.5 dB, which correspond to 70% of the transmitted power), whereas the phase difference is close to 90°. Therefore, the designed QWP metasurface acts as a polarization converter at 28.2 GHz and permits converting linear to circular polarization.

The second metasurface presented in Figure 3(b) is a HWP device designed to transmit both x-polarization and y-polarization with equal moduli and phase shift difference $|\Delta\phi| \approx 180^\circ$. With minor radius, $a = 2$ mm ($\approx\lambda/5$), and major radius $b = 2.26$ mm ($\approx\lambda/4.4$), the resonators ellipticity τ is 1.13 ($\approx\lambda/8.7$). Observing the transmitted power over the frequency band 21–28 GHz (see Figure 5) shows that the two transmission curves, corresponding to x- and y-polarization, overlap at the frequency 21.9 GHz with a transmission level close to −2.2 dB (which correspond to 60% of the transmitted power) and a phase difference of 180°. Therefore, at 21.9 GHz, the proposed HWP metasurface can change the handedness of circularly polarized wave or rotates a linear polarization by 90°.

We can explain the behavior difference between the two transmitted coefficients (T_{xx} and T_{yy}) by the effect of the asymmetric geometry of the elliptic resonators and with the nonnegligible effect of the connections.

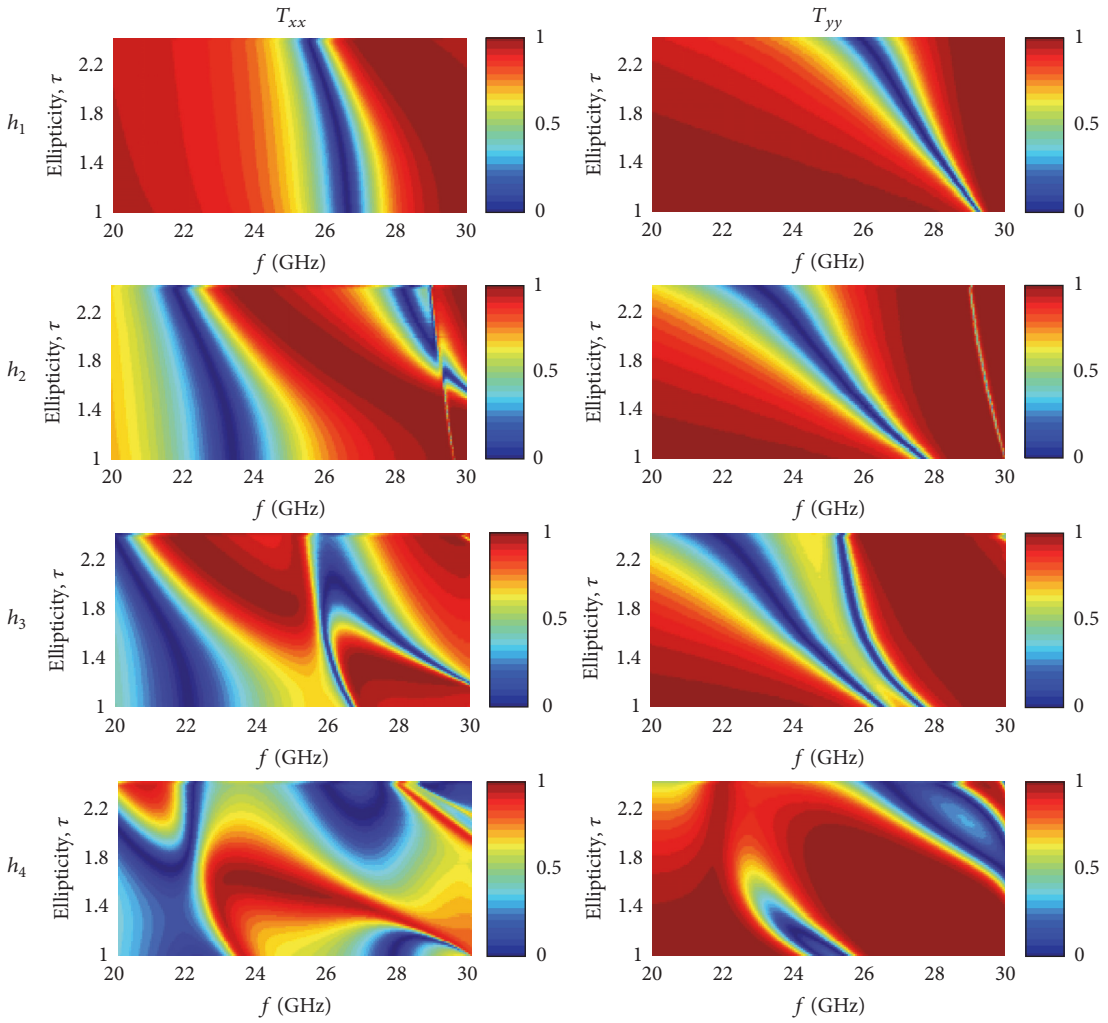

Figure 2: Continued.

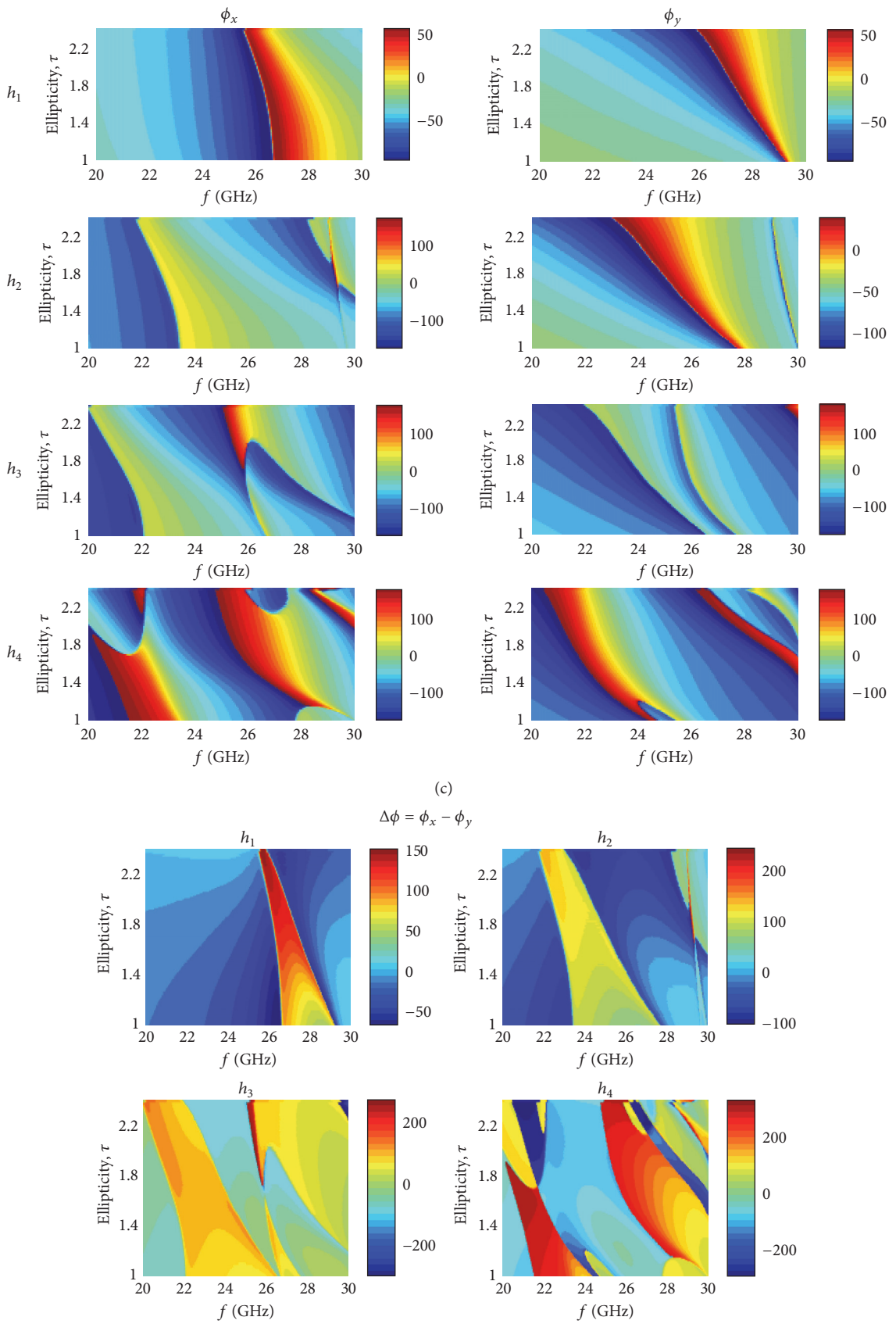

FIGURE 2: Variation, over the frequency band 20–30 GHz, of the x- and y-polarized transmission coefficients with the resonator ellipticity τ and thickness h: (a) moduli; (b) ratio between moduli; (c) phases; (d) phases difference.

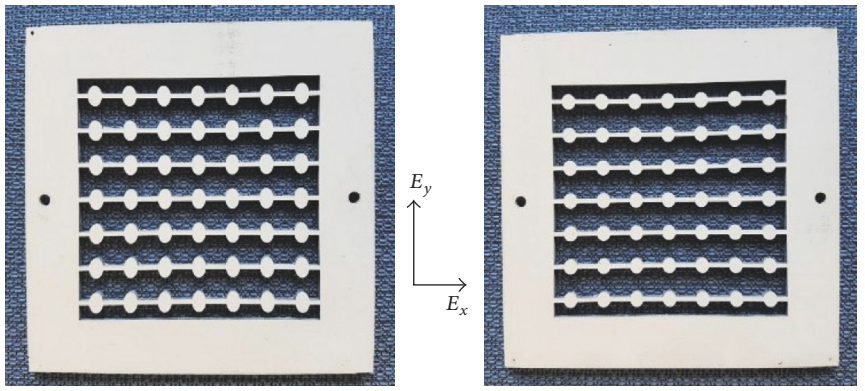

(a) (b)

Figure 3: Prototypes of the realized all-dielectric QWP (a) and HWP (b) metasurfaces.

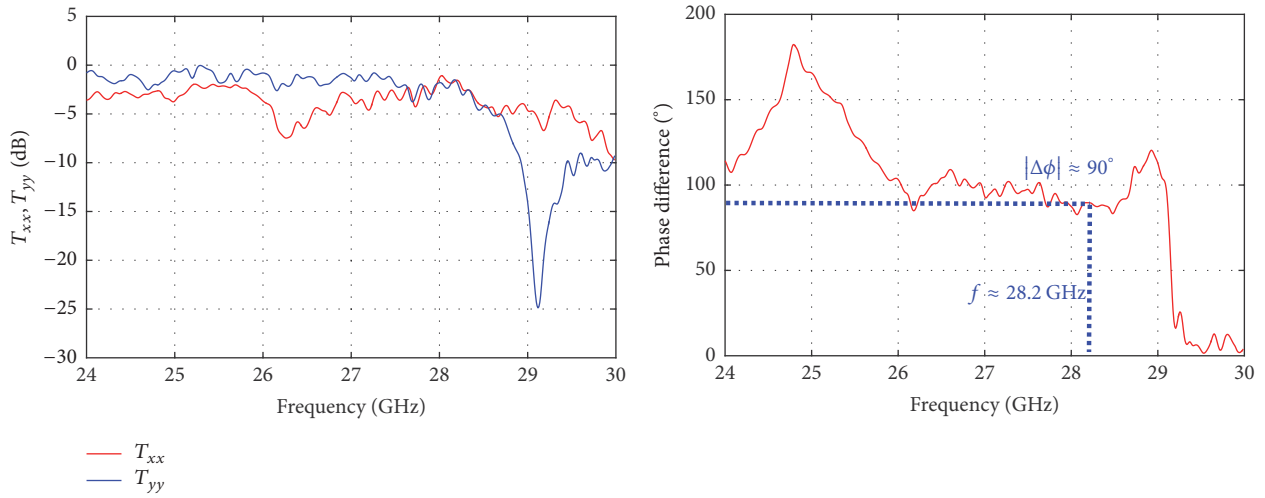

(a) (b)

Figure 4: Experimental characterization of QWP metasurface: (a) measured normalized transmitted powers T_{xx} (red) and T_{yy} (blue); (b) phase difference between x- and y-polarization.

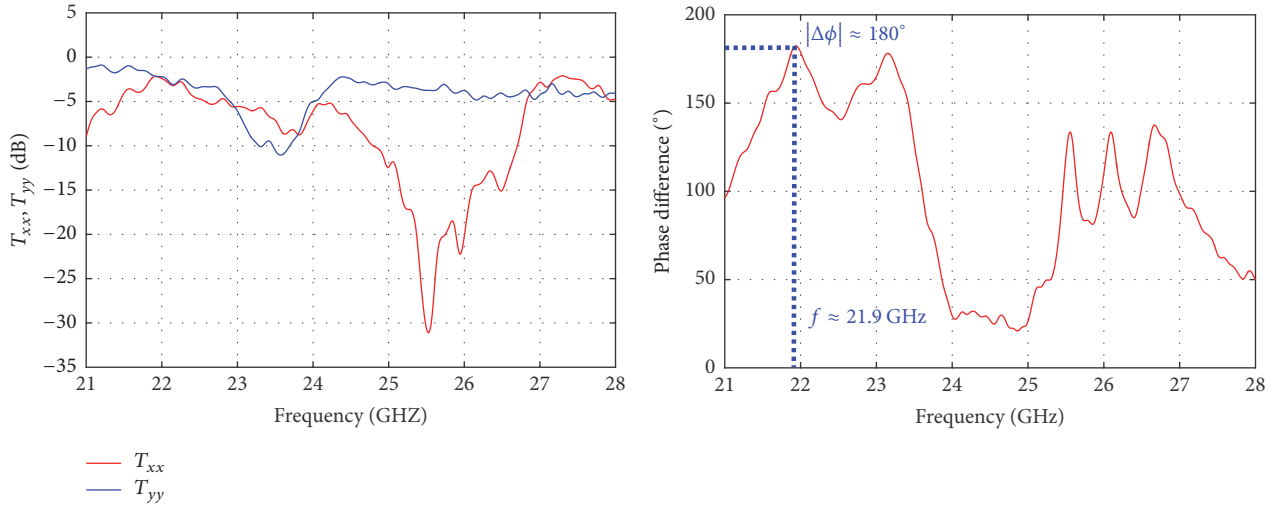

(a) (b)

Figure 5: Experimental characterization of HWP metasurface: (a) measured normalized transmitted powers T_{xx} (red) and T_{yy} (blue); (b) phase difference between x- and y-polarization.

Table 1: Main data (deduced from Figure 2) related to all-dielectric QWP and HWP metasurfaces.

h (mm)	Bandwidth (GHz)	T_{xx}	T_{yy}	QWP $\lvert\Delta\phi\rvert$	HWP $\lvert\Delta\phi\rvert$	Ellipticity (τ)
0.64	27.60–27.73	0.70–0.74	0.70–0.74	85–87	—	1.37–1.41
1.28	25.38–29.03	0.70–0.74	0.70–0.74	85–89	—	1,29–2.39
	29.18–29.23	0.72–0.77	0.72–0.84	—	177–183	1.82–1.91
1.92	—	—	—	—	—	—
2.56	20.40–30	0.70–0.96	0.70–0.99	85–95	—	1.02–2.24
	23.23–28.80	0.70–0.92	0.70–0.98	—	175–185	1.01–1.43

Table 2: Simulated and experimental results for the designed QWP and HWP metasurface.

	Simulation			Measurement		
	$T_{xx} = T_{yy}$	$\lvert\Delta\phi\rvert$	Frequency	$T_{xx} = T_{yy}$	$\lvert\Delta\phi\rvert$	Frequency
QWP	−0.6 dB	93°	26.4 GHz	−1.5 dB	90°	28.2 GHz
HWP	−0.9 dB	180°	23.3 GHz	−2.2 dB	181°	21.9 GHz

The operation bandwidths deduced from measured values extend from 25.9 GHz to 28.68 for the QWP metasurface, from 21.78 GHz to 22.15 GHz, and from 23 GHz to 23.12 GHz for the HWP metasurface. Due to losses in the structure, we have considered limits for the x- and y-transmissions coefficients modulus and phases less restrictive than simulated ones. We estimate that the obtained transmission levels are still acceptable for operation of the structure as QWP/HWP in the mentioned bands above.

Note that the transmission coefficients presented in Figures 4 and 5 have been normalized with respect to the exciting horn antenna reference transmission coefficients in the presented band.

5. Conclusion

In this paper, we have investigated numerically and experimentally the design of all-dielectric QWP and HWP metasurface operating in the microwave band 20–30 GHz. First, we have studied the effect of the resonators thickness and ellipticity on the transmission. Then we have realized the structures and measured their transmissions for both x- and y-polarized incident waves. Good agreement is obtained between simulation and measurement. It is found that the realized QWP and HWP metasurfaces operate at the frequencies 28.2 GHz and 21.9 GHz, respectively, with transmission rates of 70% and 60% of the incident power, respectively.

Conflicts of Interest

The authors declare that there are no conflicts of interest regarding the publication of this article.

Acknowledgments

This project was funded by the Deanship of Scientific Research (DSR), King Abdulaziz University, under Grant no. 25-135-35-HiCi. The authors, therefore, acknowledge technical and financial support of KAU. The authors would like to thank Professor Rabah Aldhaheri, from ECE Department, Faculty of Engineering at KAU, for his help during simulations.

References

[1] F. Capolino, *Theory and Phenomena of Metamaterials*, CRC Press, 2009.

[2] J. B. Pendry, "Negative refraction makes a perfect lens," *Physical Review Letters*, vol. 85, no. 18, pp. 3966–3969, 2000.

[3] J. B. Pendry, D. Schurig, and D. R. Smith, "Controlling electromagnetic fields," *American Association for the Advancement of Science. Science*, vol. 312, no. 5781, pp. 1780–1782, 2006.

[4] U. Leonhardt, "Optical conformal mapping," *American Association for the Advancement of Science. Science*, vol. 312, no. 5781, pp. 1777–1780, 2006.

[5] A. Silva, F. Monticone, G. Castaldi, V. Galdi, A. Alú, and N. Engheta, "Performing mathematical operations with metamaterials," *American Association for the Advancement of Science. Science*, vol. 343, no. 6167, pp. 160–163, 2014.

[6] C. L. Holloway, E. F. Kuester, J. A. Gordon, J. O'Hara, J. Booth, and D. R. Smith, "An overview of the theory and applications of metasurfaces: The two-dimensional equivalents of metamaterials," *IEEE Antennas and Propagation Magazine*, vol. 54, no. 2, pp. 10–35, 2012.

[7] C. L. Holloway, M. A. Mohamed, E. F. Kuester, and A. Dienstfrey, "Reflection and transmission properties of a metafilm: With an application to a controllable surface composed of resonant particles," *IEEE Transactions on Electromagnetic Compatibility*, vol. 47, no. 4, pp. 853–865, 2005.

[8] J. Cheng, D. Ansari-Oghol-Beig, and H. Mosallaei, "Wave manipulation with designer dielectric metasurfaces," *Optics Letters*, vol. 39, no. 21, pp. 6285–6288, 2014.

[9] H.-T. Chen, A. J. Taylor, and N. Yu, "A review of metasurfaces: physics and applications," *Reports on Progress in Physics*, vol. 79, no. 7, Article ID 076401, 2016.

[10] K. Achouri, G. Lavigne, M. A. Salem, and C. Caloz, "Metasurface spatial processor for electromagnetic remote control," *IEEE Transactions on Antennas and Propagation*, vol. 64, no. 5, pp. 1759–1767, 2016.

[11] A. Arbabi, Y. Horie, M. Bagheri, and A. Faraon, "Dielectric metasurfaces for complete control of phase and polarization with subwavelength spatial resolution and high transmission," *Nature Nanotechnology*, vol. 10, no. 11, pp. 937–943, 2015.

[12] I. Staude, A. E. Miroshnichenko, M. Decker et al., "Tailoring directional scattering through magnetic and electric resonances in subwavelength silicon nanodisks," *ACS Nano*, vol. 7, no. 9, pp. 7824–7832, 2013.

[13] M. A. Salem and C. Caloz, "Manipulating light at distance by a metasurface using momentum transformation," *Optics Express*, vol. 22, no. 12, pp. 14530–14543, 2014.

[14] K. Achouri, M. A. Salem, and C. Caloz, "General metasurface synthesis based on susceptibility tensors," *Institute of Electrical and Electronics Engineers. Transactions on Antennas and Propagation*, vol. 63, no. 7, pp. 2977–2991, 2015.

[15] K. Achouri, A. Yahyaoui, S. Gupta, H. Rmili, and C. Caloz, "Dielectric Resonator Metasurface for Dispersion Engineering," *IEEE Transactions on Antennas and Propagation*, vol. 65, no. 2, pp. 673–680, 2017.

[16] A. Yahyaoui, H. Rmili, L. Laadhar, and T. Aguili, "Numerical analysis of a metasurface based on elliptic dielectric resonators for transmission control of electromagnetic waves," in *Proceedings of the 16th Mediterranean Microwave Symposium, MMS 2016*, Abu Dhabi, UAE, November 2016.

[17] A. Yahyaoui, H. Rmili, M. Sheikh, A. Dobaie, L. Laadhar, and T. Aguili, "Half-wave and quarter-wave plates metasurfaces with elliptic dielectric resonators for microwave applications," in *Proceedings of the 16th Mediterranean Microwave Symposium, MMS 2016*, Abu Dhabi, UAE, November 2016.

[18] A. Yahyaoui, H. Rmili, M. Sheikh, A. Dobaie, L. Laadhar, and T. Aguili, "Design of All-Dielectric Half-wave and Quarter-wave Plates Microwave Metasurfaces Based on Elliptic Dielectric Resonators," *ACES Journal*, vol. 32, no. 3, pp. 229–236, March 2017.